

# An investigation of large fatigue rate in $\langle 111 \rangle_{\text{cub}}$ -oriented $\text{Pb}(\text{Mg}_{1/3}\text{Nb}_{2/3})\text{O}_3$ – $\text{PbTiO}_3$ single crystal

Y. Zhang<sup>a</sup>, Z. Xu<sup>a,\*</sup>, T. Hung<sup>a</sup>, H. Luo<sup>b</sup>, Q. Yin<sup>b</sup>

<sup>a</sup>Department of Physics and Materials Science, City University of Hong Kong, Hong Kong, PR China

<sup>b</sup>Shanghai Institute of Ceramics, Chinese Academy of Science, PR China

Received 2 September 2003; accepted 4 October 2003

## Abstract

Domain structures in  $\langle 111 \rangle_{\text{cub}}$ -oriented  $0.70\text{Pb}(\text{Mg}_{1/3}\text{Nb}_{2/3})\text{O}_3$ – $0.30\text{PbTiO}_3$  (PMN–PT) single crystal have been investigated by both optical microscopy and transmission electron microscopy (all of the orientations below will be given in terms of the prototype cubic axes, denoted by the subscript cub). Microcracking in the fatigued PMN–PT crystal samples has been observed and its forming mechanism have been analyzed in terms of domain configurations. The contribution of microcracking to the large fatigue rate in  $\langle 111 \rangle_{\text{cub}}$ -oriented PMN–PT single crystal has been identified. A new approach that is based on observed domain configuration and microcracking has been proposed to explain the large fatigue rate in the  $\langle 111 \rangle_{\text{cub}}$ -oriented PMN–PT single crystal. © 2003 Elsevier Ltd. All rights reserved.

**Keywords:** Electron microscopy; Fatigue; Perovskites; Microcracking; Domain configuration; Optical microscopy;  $\text{Pb}(\text{Mg};\text{Nb})\text{O}_3$ ;  $\text{PbTiO}_3$

## 1. Introduction

Since Kuwata et al. in the early 1980s reported the anomalously large electromechanical coupling coefficient  $K_{33}$  at room temperature in the  $\langle 001 \rangle_{\text{cub}}$  poled  $0.91\text{Pb}(\text{Zn}_{1/3}\text{Nb}_{2/3})\text{O}_3$ – $0.09\text{PbTiO}_3$  single crystal,<sup>1</sup> the feasibility of the single crystal compositions in the  $\text{Pb}(\text{Mg}_{1/3}\text{Nb}_{2/3})\text{O}_3$ – $\text{PbTiO}_3$  (PMN–PT) and  $\text{Pb}(\text{Zn}_{1/3}\text{Nb}_{2/3})\text{O}_3$ – $\text{PbTiO}_3$  (PZN–PT) solid solutions to be used as transducers and actuators has been investigated extensively in the recent several years.<sup>2–5</sup> Most of the studies have demonstrated that the  $\langle 001 \rangle_{\text{cub}}$ -oriented crystal is one of the stable engineered domain states which yield enhanced piezoelectric activity.<sup>6,7</sup> Additionally, almost identical enhancements have been observed in  $\langle 110 \rangle_{\text{cub}}$ -oriented crystals in the polydomain state.<sup>8</sup> However, in the  $\langle 111 \rangle_{\text{cub}}$ -oriented crystal the inferior strain behavior under electric field has been reported, and an instable domain configuration caused by reorientation and depoling phenomena was expected.<sup>9</sup>

Recently, large fatigue rates were found in the  $\langle 111 \rangle_{\text{cub}}$ -oriented PZN–PT ferroelectric single crystals<sup>10</sup> as well as in the  $\langle 111 \rangle_{\text{cub}}$ -oriented  $\text{Pb}(\text{Yb}_{1/2}\text{Nb}_{1/2})\text{O}_3$ – $\text{PbTiO}_3$  (PybN–PT) thin films,<sup>11</sup> while  $\langle 001 \rangle_{\text{cub}}$ -oriented samples showed a fatigue free nature. To clarify the differences in crystal orientation dependence of ferroelectric properties, research on the domain configuration of the rhombohedral phase in a variety of directions has attracted much attention.<sup>12,13</sup> Indeed, domain factors appear to be extremely important in the reproducibility and reliability of the excellent properties in these ferroelectric single crystals. It is generally believed that the degradation of ferroelectric properties, including aging and fatigue are closely related with the ferroelectric domain reorientation.

Although many studies were focused on the macroscopic properties and domain structures of the PMN–PT and PZN–PT single crystals oriented with various crystallographic directions, the  $\langle 111 \rangle_{\text{cub}}$  direction, as the polar axis of the rhombohedral phase has received little attention. In the present article, observation of the domain structure in the  $\langle 111 \rangle_{\text{cub}}$ -oriented  $0.70\text{Pb}(\text{Mg}_{1/3}\text{Nb}_{2/3})\text{O}_3$ – $0.30\text{PbTiO}_3$  single crystal has been investigated using both optical microscopy (OM) and transmission electron microscopy (TEM). The main objective of this article is to interpret the fast fatigue effects in terms of domain configuration and

\* Corresponding author.

E-mail address: [apzxx@cityu.edu.hk](mailto:apzxx@cityu.edu.hk) (Z. Xu).

microcracking, which were previously confined to domain wall pinning and switching retardation.

## 2. Experimental procedure

0.70Pb(Mg<sub>1/3</sub>Nb<sub>2/3</sub>)O<sub>3</sub>–0.30PbTiO<sub>3</sub> single crystals with  $\langle 001 \rangle_{\text{cub}}$  and  $\langle 111 \rangle_{\text{cub}}$  orientations were provided by Shanghai Institute of Ceramics. The above composition corresponds to a rhombohedral ferroelectric phase that is close to the morphotropic phase boundary (MPB) at room temperature. The samples were prepared from the  $\{001\}_{\text{cub}}$  and  $\{111\}_{\text{cub}}$  plates by ultrasonically cutting to 3 mm discs and mechanically polishing to about 400  $\mu\text{m}$  in thickness. The flat surfaces were sputtered with gold leaving a rim of 300  $\mu\text{m}$  uncovered. During fatigue measurements, the samples were immersed in silicone oil to prevent arcing. A ferroelectric testing system RT Precision Pro (Radiant technologies, Inc.) equipped with intelligent high voltage interface (HVI), was used to measure the polarization hysteresis and supply fatigue electric field with sinusoidal waveform.

For in situ TEM experiment, great care was taken to prepare the TEM foils. Details of the in situ TEM specimen preparation can be found elsewhere.<sup>14</sup> The specimens were examined using a Philips CM20 at 200 kV. In addition, a Trek Model 609E-6-FG high-voltage function generator was used to provide the needed electric field with different waveforms and frequencies for in situ TEM observation.

## 3. Results and discussion

Fig. 1 shows the fatigue behavior at room temperature for  $\langle 001 \rangle_{\text{cub}}$ - and  $\langle 111 \rangle_{\text{cub}}$ -oriented PMN–PT crystal samples. The coercive field of the  $\langle 001 \rangle_{\text{cub}}$ -

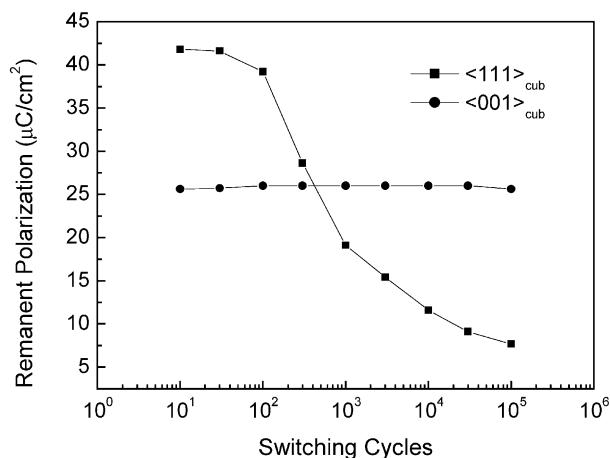


Fig. 1. Fatigue behavior of  $\langle 001 \rangle_{\text{cub}}$ - and  $\langle 111 \rangle_{\text{cub}}$ -oriented PMN–PT single crystal samples.

and  $\langle 111 \rangle_{\text{cub}}$ -oriented samples were 2.5 and 3.5 kV/cm, respectively. A bipolar cyclic field with an amplitude of 7.0 kV/cm and frequency of 10 Hz was applied to both samples during fatigue measurements. The  $\langle 001 \rangle_{\text{cub}}$ -oriented sample shows a fatigue free behavior, as expected. On the other hand, a quick decay of the remanent polarization between 10<sup>2</sup> and 10<sup>4</sup> switching cycles is evident for the  $\langle 111 \rangle_{\text{cub}}$ -oriented sample. This fast fatigue rate is similar to that observed in Pb(Zn<sub>1/3</sub>Nb<sub>2/3</sub>)O<sub>3</sub>–PbTiO<sub>3</sub> crystal samples.<sup>10,15</sup>

After the fatigue measurements, the crystal samples were examined by polarized optical microscopy in a transmission mode. No visible damage in the  $\langle 001 \rangle_{\text{cub}}$ -oriented sample was detected, while many elliptical and edge microcracks were found in the  $\langle 111 \rangle_{\text{cub}}$ -oriented sample, as shown in a representative optical image in Fig. 2. Fig. 2 is the typical crack pattern observed from a fatigued  $\langle 111 \rangle_{\text{cub}}$ -oriented sample showing dense elliptical microcracks around the flaws. This kind of microcracks has not previously been reported in PMN–PT single crystals, but it has been observed in many macroscopic fracture mechanical experiments of single crystal specimens. Their formation can be interpreted as the stress gradient around the vicinity of a flaw. The singularity of the local field is concentrated at the flaw, this can give rise to a region of enhanced stresses. Once the domain system can not accommodate such stresses, the type of elliptical microcrack forms. Another kind of microcracks called edge microcrack is also dominant in the observed region. It is known that its initiation and growth are caused by the strain incompatibility between the electrically active (electroded) area and inactive (unelectroded) area.<sup>16</sup>

To account for the large fatigue rate in the  $\langle 111 \rangle_{\text{cub}}$ -oriented samples, the domain structure of the  $\{111\}_{\text{cub}}$  single crystal plate was examined by using both OM and TEM. Fig. 3 is an OM image showing typical domain configuration. A hierarchy of domains

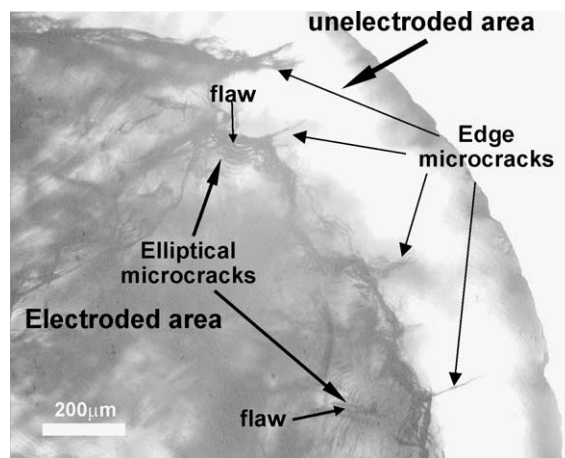


Fig. 2. OM image of a fatigued  $\langle 111 \rangle_{\text{cub}}$ -oriented PMN–PT single crystal sample.

in the single crystal sample is evident. The similar hierarchy of domains was observed by TEM also, as illustrated in Fig. 4 at a higher resolution. The inset in Fig. 4 is a corresponding  $\langle 111 \rangle_{\text{cub}}$  selected area electron diffraction pattern recorded from the examined area. The observed domain width ranges from  $\sim 20$  nm (by TEM) to  $\sim 30$   $\mu\text{m}$  (by OM) and the domain walls intersect each other at either  $60^\circ$  or  $120^\circ$ , as expected from a rhombohedral structure. The suggested configuration of the  $\{110\}$ -type and  $\{001\}$ -type ferroelectric domain walls viewed along  $\langle 111 \rangle_{\text{cub}}$  direction is shown in Fig. 5. Although the  $\{110\}$ -type and  $\{001\}$ -



Fig. 3. OM image showing the domain configuration in a  $\langle 111 \rangle_{\text{cub}}$ -oriented PMN-PT single crystal sample.

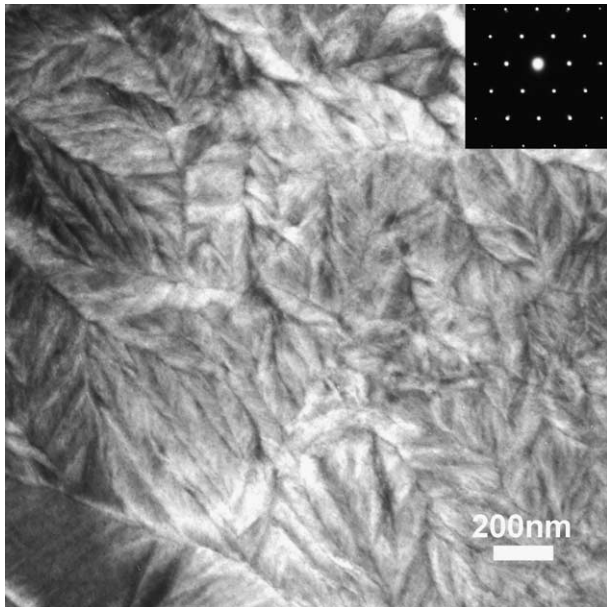


Fig. 4. Bright-field TEM image of the ferroelectric domains in a  $\langle 111 \rangle_{\text{cub}}$ -oriented PMN-PT single crystal specimen. The inset is the corresponding selected area electron diffraction pattern.

type domain walls are not discernible from the pictures due to the superimposed effect, the short white and black strips in Fig. 3 correspond to antiparallel  $180^\circ$  domains.

By considering the domain structure viewed along  $\langle 111 \rangle_{\text{cub}}$  direction, the cracks observed in Fig. 2 can be explained by the strain mismatch between the antiparallel domains. In a simplified model shown in Fig. 6, the application of the electric field will make one domain grow and the other shrink along field direction, the difference in strain between the two domains leads to the maximum strain mismatch, thus generating mechanical stress on the domain walls. Therefore, microcracks along the domain wall will initiate to relieve some of the stress.

In order to obtain further evidence for the easily occurring microcracking, in situ TEM analysis was carried out on the  $\langle 111 \rangle_{\text{cub}}$  and  $\langle 001 \rangle_{\text{cub}}$ -oriented single crystal samples. Fig. 7 shows a microcracking pattern viewed along  $\langle 111 \rangle_{\text{cub}}$  direction after an electric field has been applied for a while. An irregular microcracking path along the domain boundaries, numerous delamination microcracks and crack kinking are evident. This picture is of interest because not only

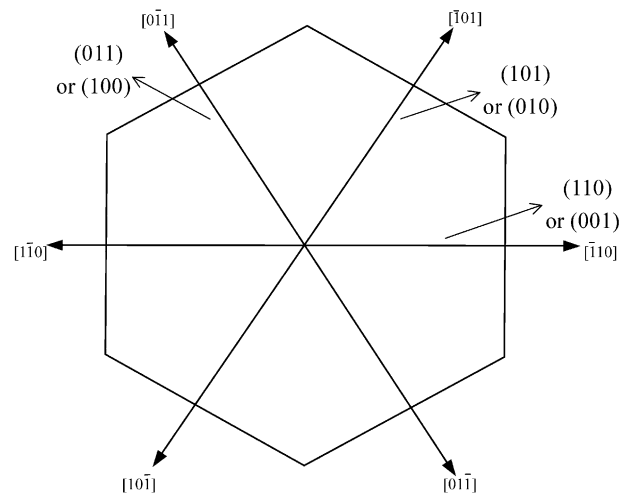


Fig. 5. Schematic illustration of  $\{110\}_{\text{cub}}$ -type and  $\{001\}_{\text{cub}}$ -type ferroelectric domain walls of rhombohedral phase viewed along  $\langle 111 \rangle_{\text{cub}}$ .

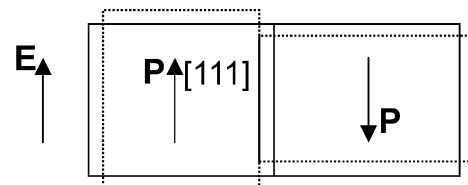


Fig. 6. Simplified model showing the effect of an applied electric field on antiparallel  $180^\circ$  domains in  $\langle 111 \rangle_{\text{cub}}$ -oriented specimens, where the applied field is parallel to the polarization direction.

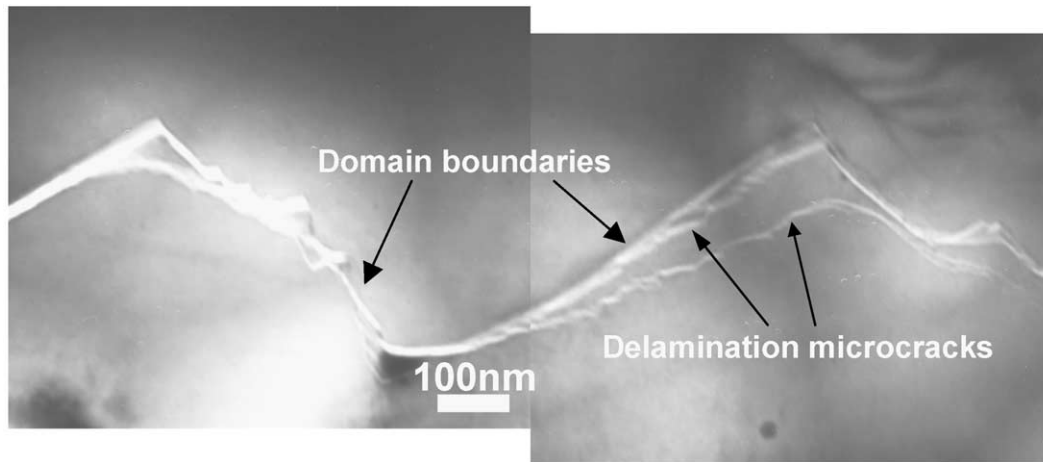


Fig. 7. Bright-field TEM image showing the microcracking behavior observed in a  $\langle 111 \rangle_{\text{cub}}$ -oriented PMN–PT single crystal specimen.

does it show different kinds of microcracks, but also it is proved that high tensile stress caused by the domain switching is located along the domain wall in the  $\langle 111 \rangle_{\text{cub}}$  oriented single crystal samples. Some domains in the  $(111)_{\text{cub}}$  plane will experience a higher out-plane strain since their spontaneous polarization vectors are perpendicular to the observed plane. Consequently, a very high strain incompatibility and accompanying stress between the antiparallel domain are generated under the fatigue electric fields. Moreover, it can be seen from Fig. 4 that the domain walls display a wiggly feature and have complexity in the geometry, thus indicating that the domain walls are in an anisotropic stress condition. Upon application of a fatigue electric field, the anisotropy in the single crystal disturbs the microcrack tip stress field, the microcrack propagation experiences curving and kinking. In addition, our in situ TEM experiment has also found that after the fatigue, the  $\langle 111 \rangle_{\text{cub}}$ -oriented single crystal specimens have a considerable higher microcrack density than the  $\langle 001 \rangle_{\text{cub}}$ -oriented single crystal specimens do.

#### 4. Conclusions

The large fatigue rate in the  $\langle 111 \rangle_{\text{cub}}$ -oriented  $0.70\text{Pb}(\text{Mg}_{1/3}\text{Nb}_{2/3})\text{O}_3\text{--}0.30\text{PbTiO}_3$  single crystal has been confirmed. The domain structures of  $(111)$  PMN–PT crystal samples have been examined using both optical microscopy and transmission electron microscopy. The contribution of microcracking to the reduction of remanent polarization was identified and the forming mechanism of microcracks has been analyzed. A new approach that is based on observed domain configuration and microcracking has been proposed to explain the large fatigue rate in the  $\langle 111 \rangle_{\text{cub}}$ -oriented PMN–PT single crystal.

#### Acknowledgements

This work was supported by a grant from the Research Grant Council of the Hong Kong Special Administrative Region, China [Project No. 9040643]. One of the authors Dr. Zhang is grateful to Dr. D.C. Lupascu at Darmstadt University of Technology, Germany for helpful discussions.

#### References

1. Kuwata, J., Uchino, K. and Nomura, S., Dielectric and piezoelectric properties of  $0.91\text{Pb}(\text{Zn}_{1/3}\text{Nb}_{2/3})\text{O}_3\text{--}0.09\text{PbTiO}_3$  single crystals. *Jpn. J. Appl. Phys., Part 1*, 1982, **21**(9), 1298–1302.
2. Park, S. E. and Shrout, T. R., Characteristics of relaxor-based piezoelectric single crystals for ultrasonic transducers. *IEEE Trans. UFFC*, 1997, **44**(5), 1140–1147.
3. Saitoh, S., Kobayashi, T., Harada, K., Shimanuki, S. and Yamashita, Y., Simulation and fabrication process for a medical phased array ultrasonic probe using a  $0.91\text{Pb}(\text{Zn}_{1/3}\text{Nb}_{2/3})\text{O}_3\text{--}0.09\text{PbTiO}_3$  single crystal. *Jpn. J. Appl. Phys., Part 1*, 1998, **37**(5B), 3053–3057.
4. Ritter, T., Geng, X. C., Shung, K. K., Lopath, P. D., Park, S. E. and Shrout, T. R., Single crystal PZN/PT-polymer composites for ultrasound transducer applications. *IEEE Trans. UFFC*, 2000, **47**(4), 792–800.
5. Viehland, D., Ewart, L., Powers, J. and Li, J. F., Stress dependence of the electromechanical properties of  $\langle 001 \rangle$ -oriented  $\text{Pb}(\text{Mg}_{1/3}\text{Nb}_{2/3})\text{O}_3\text{--PbTiO}_3$ . *J. Appl. Phys.*, 2001, **90**(5), 2479–2483.
6. Park, S. E. and Shrout, T. R., Ultrahigh strain and piezoelectric behavior in relaxor based ferroelectric single crystals. *J. Appl. Phys.*, 1997, **82**(4), 1804–1811.
7. Saitoh, S., Kobayashi, T., Harada, K., Shimanuki, S. and Yamashita, Y., Forty-channel phased array ultrasonic probe using  $0.91\text{Pb}(\text{Zn}_{1/3}\text{Nb}_{2/3})\text{O}_3\text{--}0.09\text{PbTiO}_3$  single crystal. *IEEE Trans. UFFC*, 1999, **46**(1), 152–157.
8. Viehland, D., Amin, A. and Li, J. F., Piezoelectric instability in  $\langle 011 \rangle$ -oriented  $\text{Pb}(\text{Bi}_{1/3}\text{B}_{2/3})\text{O}_3\text{--PbTiO}_3$  crystals. *Appl. Phys. Lett.*, 2001, **79**(7), 1006–1008.
9. Liu, S. F., Park, S. E., Shrout, T. R. and Cross, L. E., Electric field dependence of piezoelectric properties for rhombohedral



- 0.955Pb(Zn<sub>1/3</sub>Nb<sub>2/3</sub>)O<sub>3</sub>–0.045PbTiO<sub>3</sub> single crystals. *J. Appl. Phys.*, 1999, **85**(5), 2810–2814.
10. Takemura, K., Ozgul, M., Bornand, V., Trolier-Mckinstry, S. and Randall, C. A., Fatigue anisotropy in single crystal Pb(Zn<sub>1/3</sub>Nb<sub>2/3</sub>)O<sub>3</sub>–PbTiO<sub>3</sub>. *J. Appl. Phys.*, 2000, **88**(12), 7272–7277.
  11. Bornand, V., Trolier-McKinstry, S., Takemura, K. and Randall, C. A., Orientation dependence of fatigue behavior in relaxor ferroelectric-PbTiO<sub>3</sub> thin films. *J. Appl. Phys.*, 2000, **87**(8), 3965–3972.
  12. Mulvihill, M. L., Cross, L. E., Cao, W. W. and Uchino, K., Domain-related phase transitionlike behavior in lead zinc niobate relaxor ferroelectric single crystals. *J. Am. Ceram. Soc.*, 1997, **80**(6), 1462–1468.
  13. Abplanalp, M., Barosova, D., Bridenbaugh, P., Erhart, J., Fousek, J., Gunter, P., Nosek, J. and Sulc, M., Scanning force microscopy of domain structures in Pb(Zn<sub>1/3</sub>Nb<sub>2/3</sub>)O<sub>3</sub>–8%PbTiO<sub>3</sub> and Pb(Mg<sub>1/3</sub>Nb<sub>2/3</sub>)O<sub>3</sub>–29%PbTiO<sub>3</sub>. *J. Appl. Phys.*, 2002, **91**(6), 3797–3804.
  14. Xu, Z., In situ TEM study of electric field-induced microcracking in piezoelectric single crystals. *Mater. Sci. and Eng. B*, 2003, **99**, 106–111.
  15. Ozgul, M., Takemura, K., Trolier-Mckinstry, S. and Randall, C. A., Polarization fatigue in Pb(Zn<sub>1/3</sub>Nb<sub>2/3</sub>)O<sub>3</sub>–PbTiO<sub>3</sub> ferroelectric single crystals. *J. Appl. Phys.*, 2001, **89**(9), 5100–5106.
  16. dos Santos e Lucato, S. L., Lupascu, D. C. and Roedel, J., Crack initiation and crack propagation in partially electroded PZT. *J. Eur. Ceram. Soc.*, 2001, **21**, 1425–1428.